Performance of the Cable-in-Conduit Conductors for Super-X Test Facility

Chao Dai, Yu Wu, Yi Shi, Kamil Sedlak, Hugo Bajas, Arend Nijuis, Qiangwang Hao, Houxiang Han, YunHao Liu, Arnaud Devred, *Senior Member, IEEE*, and Jinggang Qin

***Abstract*—Following the conceptual design, the engineering design of the dc magnet and cable-in-conduit conductor (CICC) for the Super-X test facility has been done in 2021. Totally three types of conductors with different structures were designed for the three pairs of coils in the dc magnet, respectively. High-J_c Nb_3Sn strand (J_c ~2200 A/mm^2 at 12 T, 4.2 K) was applied to high field and middle field coils for reducing the radius of the dc magnet. In order to qualify if the designed parameters of the conductors could fulfill the performance criteria, three pairs of short samples have been manufactured and tested successfully in the SULTAN facility at SPC, Switzerland. Test results and analysis show that dc performance of the three types of conductors can meet the design criteria. The conductor qualification process including the sample preparation, test results, and analysis are presented in this article. The HFC and LFC conductors exhibit different ac loss behavior to the MFC conductor, which is discussed in the article.**

***Index Terms*—AC loss behavior, cable-in-conduit-conductors, current sharing temperature, electromagnetic load cycle, Super-X.**

I. Introduction

TEST facility named "Super-X" is being built in the Institute of Plasma Physics, CAS (ASIPP) with the aim to provide the test conditions for large-size, high field, and high current superconductors contributing to the future fusion reactor and other large-scale superconducting magnets. This test facility is a subtask of the "Comprehensive Research facility for Fusion Technology" (CRAFT) project, which was launched in 2019, supported by the Chinese government.

The Super-X test facility is designed to generate a maximum dc field B_d= 15 T over a length of 550 mm with a homogeneity of >95%. The cross-sectional dimension of the test well is 10 cm × 16 cm. Out of the test well is an ac coil, which can generate an ac field of ±0.4 T with a frequency f<10 Hz, perpendicular to both, the dc field direction and sample axis. The testing current of up to 100 kA is provided by a superconducting transformer. The conceptual design and engineering design of the Super-X test facility have been completed in 2020 and 2022, respectively [1], [2], [3]. Fig. 1 shows the profile of the test facility.

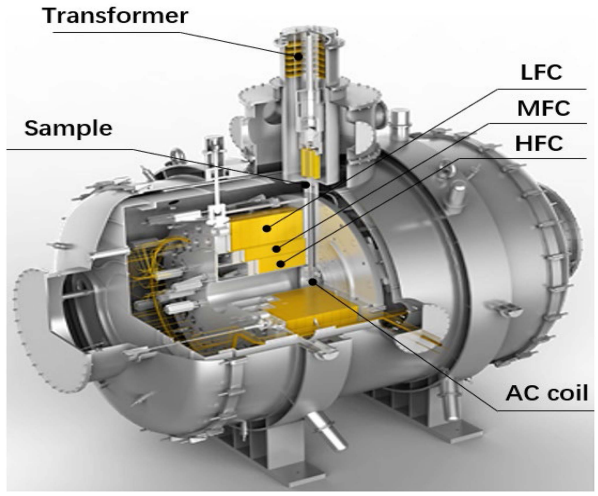

Fig. 1. Profile and sectional view of the super-X test facility.

The dc magnet of the Super-X test facility consists of three pairs of split solenoid coils, which are high-field coils (HFC), mid-field coils (MFC), and low field coils (LFC), as shown in Fig. 1. The HFC and MFC are series-connected, the operating parameters of the dc magnet are listed in Table I. Three types of cable-in-conduit conductors (CICC) have been designed for the HFC, MFC, and LFC, respectively, all of them are with rectangular cross-section, different dimensions, and cable layouts. The preliminary design of the conductors was completed in 2019 and reported in [2]. After slight optimization, three pairs of prototype conductors have been manufactured and tested in

Manuscript received 30 July 2022; revised 17 November 2022; accepted 21 November 2022. Date of current version 6 December 2022. This work was supported in part by the Comprehensive Research Facility for Fusion Technology Program of China under Contract 2018-000052-73-01-001228 and in part by National Natural Science Foundation of China under Grant 51977207. This article was recommended by Associate Editor V. Selvamanickam. *(Corresponding author: Yi Shi.)*

Chao Dai is with the Institute of Plasma Physics, CAS, Hefei 230031, China, and also with the Huainan New Energy Research Center, Huainan 232000, China (e-mail: dc@ipp.ac.cn).

Yu Wu, Yi Shi, Qiangwang Hao, Houxiang Han, and Jinggang Qin are with the Institute of Plasma Physics, CAS, Hefei 230031, China (e-mail: wuyu@ipp.ac.cn; shiyi@ipp.ac.cn; haoqw@ipp.ac.cn; hhx@ipp.ac.cn; qinjg@ipp.ac.cn).

Kamil Sedlak and Hugo Bajas are with the Swiss Plasma Center, École Polytechnique Fédérale de Lausanne, CH-1211 Geneva, Switzerland (e-mail: kamil.sedlak@psi.ch; hugues.bajas@psi.ch).

Arend Nijuis is with the Energy, Materials and Systems, Faculty of Science and Technology, University of Twente, 7500AE Enschede, The Netherlands (e-mail: a.nijhuis@utwente.nl).

YunHao Liu is with the University of Sciences and Technology of China, Hefei 230026, China (e-mail: yunhao.liu@ipp.ac.cn).

Arnaud Devred is with the CERN,TE Department, CH-1211 Geneva, Switzerland (e-mail: arnaud.devred@cern.ch).

Color versions of one or more figures in this article are available at https://doi.org/10.1109/TASC.2022.3224589.

Digital Object Identifier 10.1109/TASC.2022.3224589

TABLE I
OPERATING PARAMETERS OF THE DC MAGNET

	HFC	MFC	LFC
Operating current [kA]	8.5	8.5	14.0
Maximum field [T]	15.70	12.80	10.56
Operating temperature [K]	4.5	4.5	4.5

TABLE II
SCALING PARAMETERS OF THE THREE TYPES OF Nb_3Sn STRAND

	M2007	B2024	ITER Nb_3Sn
C_a1	38.00	45.00	49.00
C_a2	2.60	6.00	0.300
$\epsilon_{0,a}$	0.240%	0.20%	0.312%
ϵ_m	-0.407%	-0.18%	-0.059%
$\mu_0 H_{c2}(0)$ (T)	29.17	28.77	33.24
$T_{cm}(0)$ (K)	15.92	15.65	16.34
$C1$ (A·T)	47700	53000	25038
p	0.5	0.5	0.593
q	2.0	2.0	2.156

the SULTAN facility at SPC, Switzerland, in 2022. The details of the test results are presented in following sections.

II. SUPERCONDUCTING STRAND

Two grades of Nb_3Sn strand are used for manufacturing of the conductors, which are high-J_c Nb_3Sn strand for the HFC and MFC conductors and ITER-like Nb_3Sn strand for the LFC conductor. For the high-J_c Nb_3Sn, the type M2007 from Bruker-OST and type B2024 from WST are the candidates. The critical current densities of both types of high-J_c Nb_3Sn strand are above 2000 A/mm^2 at 12 T, 4.2 K. The OST M2007 Nb_3Sn strand has been used in multiple projects such as EDIPO [4], [5] and SHMFF outer coil [6]. The B2024 Nb_3Sn strand from WST is a newly developed strand for this project. The ITER-like Nb_3Sn strand is provided by WST, which is optimized on the basis of ITER TF Nb_3Sn strand, the critical current density is above 900 A/mm^2 at 12 T, 4.2 K. The diameter of all strands and the Cu to non-Cu ratio are selected to be 0.82 mm and 1.0, respectively. The hysteresis loss (Q_h) of high-J_c Nb_3Sn strand is much higher than that of ITER-like Nb_3Sn strand, but since there is no ac operation condition for this magnet, it is considered acceptable. Another issue of high-J_c Nb_3Sn strand is the thermomagnetic instability, but the single-strand operating currents of the HFC and MFC conductors are much lower than the quench current [7] associated with the flux jumps in low magnetic field, i.e., the strand operates in the safe region.

For assessing conductor performance, the critical performance of the strands versus field, temperature, and strain have been measured at University of Twente and University of Geneva. The measured data are fitted by the deviatoric strain model [8] and the resulting scaling parameters are listed in Table II. Fig. 2 shows the comparison of the strain dependence

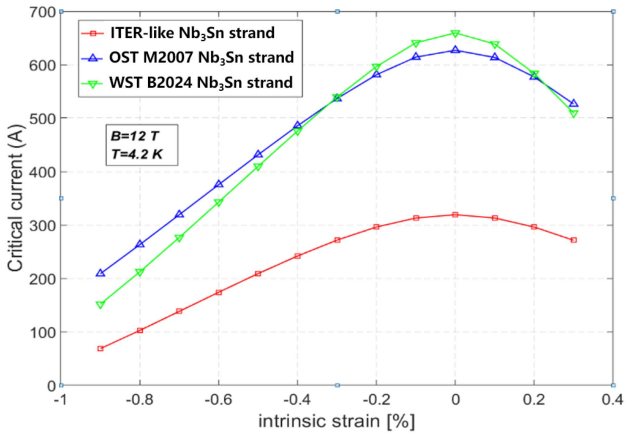

Fig. 2. Comparison of the strain dependence of the critical current for the three types of Nb_3Sn strand at 12 T, 4.2 K.

TABLE III
MAIN PARAMETERS OF THE CONDUCTORS

	HFC	MFC	LFC
Strand type	High-J_c Nb_3Sn	High-J_c Nb_3Sn	ITER-like Nb_3Sn
Strand diam. (mm)	0.82 mm (Cr-plated)		
Cu: Non-Cu	1.0		
Cable Pattern	3sc×4×5×6	(1sc+2cu)×4×4×5	(1sc+2cu)×4×5×6
Twist pitch sequence	62/140/190/230 mm	56/95/140/210 mm	62/140/190/230 mm
Number of SC strands	360	80	120
Number of Cu strands	0	160	240
Void Fraction (%)	~30%	~30%	~30%
Cond. Dimension	30.6 x 13.9 mm	24.6 x 14.8 mm	33.1 x 15.2 mm
Inner corner radius	2 mm	2 mm	3 mm
Jacket thickness	1.8 mm	2.5 mm	2.6 mm

of the critical currents for the three types of strands at 12 T. From the figure, it can be seen that the WST B2024 strand is more sensitive to strain.

III. CONDUCTOR PERFORMANCE QUALIFICATION

A. Conductor Layout

The CICC cable patterns of the three types of conductors are similar to that in the conceptual design [2]. The cable pattern of the HFC conductor and LFC conductor is kept identical as it reduced the engineering and manufacturing complexity. The geometric features of the cross-section, i.e., the dimensions, jacket thickness, and the aspect ratios, of the three types of conductors were adjusted slightly to adapt the updates of the coil structures. The conductor layouts have been frozen in February 2022 and the updated conductor parameters are listed in Table III.

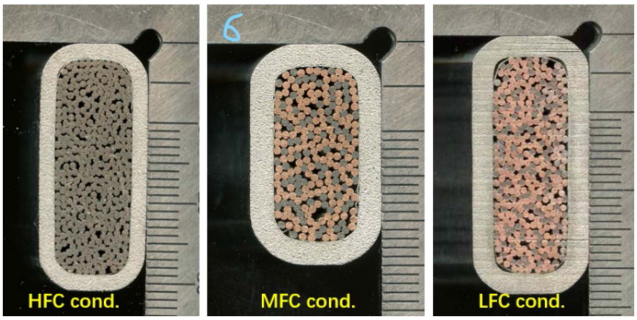

Fig. 3. Cross-sections of the three types of conductors.

B. Experimental Setup

In total, three pairs of conductors have been manufactured in 2021 to be used for SULTAN samples. The two legs of the LFC conductor sample are with the same type of strand, but for the HFC and MFC conductor samples, the two legs of each sample are prepared with different types of Nb_3Sn strand, i.e., the left leg is made of OST M2007 Nb_3Sn strand and the right leg is made of WST B2024 Nb_3Sn strand, for making a comparison. The conductor cross-sections are shown in Fig. 3.

The test campaign includes the dc test, ac test, and MQE test, in this article, only the dc and ac test results are reported.

In the dc test, cyclic electromagnetic (EM) loading (IxB, I is the transport current of the sample, and B is the superposition of the background field and the self-field of the sample) was performed to investigate if the conductor performance would be affected by the EM load up to a number of 1000 EM cycles (the estimated EM and Warm-Up-Cool-Down (WUCD) cycles are 300 and 60, respectively). Because the maximum applied background field provided by the SULTAN facility is limited to 10.8 T, and taking the conductor self-fields into consideration, the maximum field and EM load on the HFC and MFC conductor samples are lower than for their operation conditions. The conductors can nevertheless be tested at the operating load by increasing the transport current to reach the equivalent EM load, and then the conductor performance of the samples in real operating conditions can be assessed by combining the measured data of the conductors and the scaling laws of the strands. Except for the tests with anticipated operating conditions, overload tests were performed on all samples for exploring the possible critical point of irreversible performance change. In order to make sure that the current sharing temperature (T_{cs}) of each sample is above 4.5 K (helium inlet temperature of the SULTAN sample), the maximum EM load was restricted to 150% of the normal operation EM load.

The AC losses of the conductors were measured before and after EM & WUCD cycles, at 0 and 9 T, with or without transport current. The frequency ranges from 0.2 to 7.0 Hz.

The test campaigns of the conductor samples were performed in the following main steps:

1) Instrumentation check.
2) AC losses tests: before cycling at 0 T / 0 kA, 9 T / 0 kA, 9 T / 8 kA (MFC and HFC conductor) or 13 kA (LFC conductor).
3) Initial critical current (I_c) and T_{cs} runs.
4) T_{cs} runs with cyclic EM loading & WUCD, T_{cs} runs at the cycle of # 50, #150, #500, #1000, WUCD.
5) AC losses tests: after cycling.
6) Overload tests at 135% and 150% of the normal operation load.

C. Test Results and Analysis

1) T_{cs} Evolution With EM Cyclic Loading and WUCD: The T_{cs} value and evolution with EM cyclic loading and WUCD is the most important result in the conductor and magnet performance assessment. For the HFC and MFC conductors, the normal cyclic EM load applied on the conductor (100% EM load) are 10.85 T $\times$ 11.1 kA and 10.85 T $\times$ 9.15 kA, respectively, of which the transport currents are increased to attain the equivalent operating EM loads of the conductors. For the LFC conductor, the normal cyclic EM load is similar to its operating condition. The self-field (0.21 T/10 kA for HFC and LFC conductors and 0.26 T/10 kA for MFC conductor) of the SULTAN sample is considered in test condition setup. One WUCD cycle was performed after the 100% EM load cycles were finished. In overload tests, T_{cs} was measured at 135% load and back to 100% load, after 200 cycles with 135% load. Then, the same sequence was repeated with 150% load. These tests aim to investigate whether the overloads would cause an irreversible change on the conductor performance. Fig. 4 shows T_{cs} evolution with the EM cyclic loading and WUCD of the three types of conductors.

It can be seen from the plots that no degradation in performance is observed with EM cycling at nominal loading. Even when the overloads were applied, the performance of two out of the three types of conductors remained stable. One point of concern could be the observed decrease of T_{cs} (about 0.1 K) after the WUCD cycle and then remained stable during the following EM cycles for the left leg of MFC conductor, which is manufactured with M2007 strand. Meanwhile, a visible increase of T_{cs} for both legs of the HFC conductor sample can be observed after the overload cycling. A possible reason for these T_{cs} changes is that the strain state of the cables was changed by the EM and WUCD cycle.

2) Assessment of the Effective Strain: In order to extrapolate T_{cs} values of HFC and MFC conductors for their operating conditions, a parameter referred to as the effective strain of the conductor is assessed. The effective strain is used as a simplified single parameter in conductor performance analysis, which neglects the complex strain distribution inside the conductor. The effective strain can be fitted as a free parameter in (1), in which another free parameter is the *n*-value of the conductor and E_{calc} is the calculated electrical field. The detailed calculation process can be found in [9]. Fig. 5 shows the simulated *E-T* curve compared with the measured data

$$E_{calc} = \frac{E_c}{A_{cable}} \int \left(\frac{J}{J_c(B, T, \varepsilon_{eff})} \right) n_{dA}. \tag{1}$$

Fig. 6 shows the effective strain as a function of the applied transverse EM load for the three types of conductors. It can be seen that the effective strains of the conductors are independent of the transverse EM load, which indicates that the EM load on such level does not affect the conductor performance and the

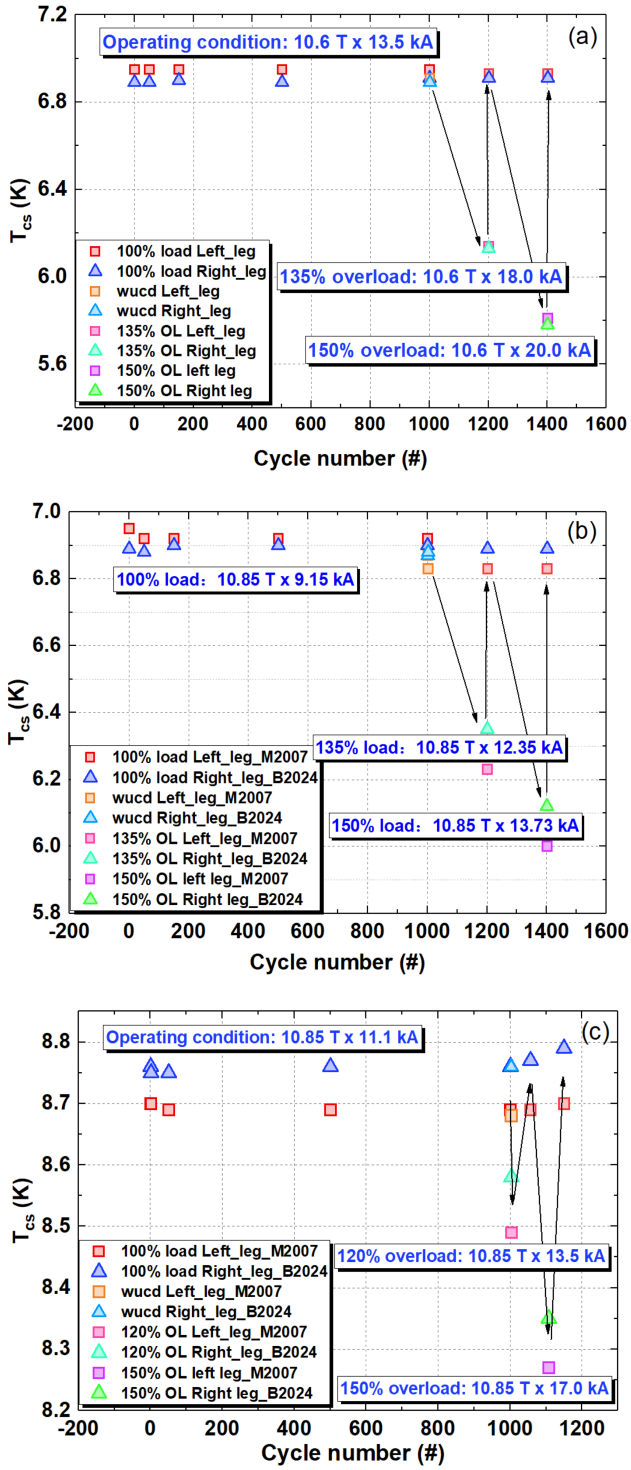

Fig. 4. T_{cs} evolution with EM and WUCD cycles under nominal load and overload of LFC (a) MFC, (b) and HFC, (c) conductors.

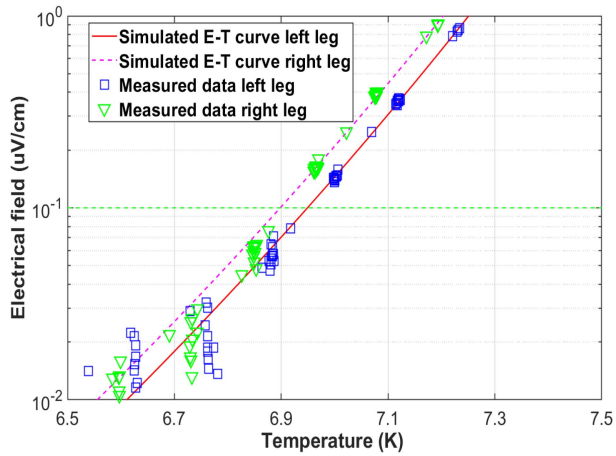

Fig. 5. Comparison between *E-T* simulated curve and measured data of one T_{cs} run.

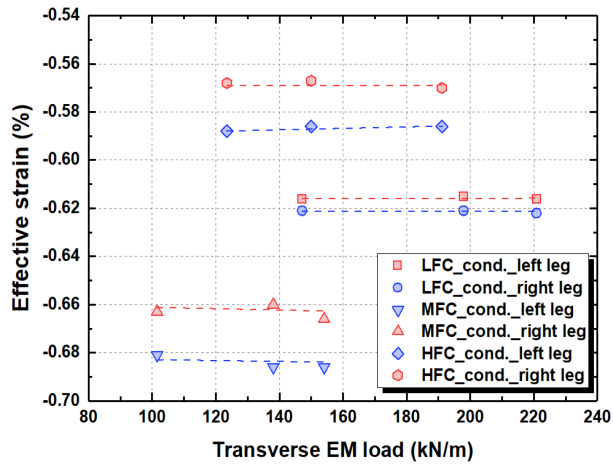

Fig. 6. Effective strain as a function of the applied transverse EM load for the three types of conductors.

thermal contraction dominates the strain state of the conductors. The MFC conductor shows much higher effective compressive strain compared with the HFC and LFC conductors. This may be attributed to the different structures of the conductors, especially concerning the ratio between superconducting and nonsuperconducting cross-sectional area within the conductor. The strain of the conductors caused by the thermal contraction was assessed with the thermal contraction coefficient of each component in the conductor [10], and compared with the measured effective strains, which are shown in Fig. 7.

The measured effective strain agrees well with the estimated thermal strains, the strain transmission ratio between the jacket and cable ranges from 85–95%.

Based on the assessed effective strains, T_{cs} of the HFC and MFC conductors for their operating conditions can be extrapolated to be 6.01 K and 5.97 K, respectively, meanwhile the measured T_{cs} of LFC conductor is around 6.9 K, which indicates that the performances of the three types of conductors can meet the specification of T_{cs}>5.7 K.

3) AC Losses: The ac losses of the three types of conductors were measured before and after cyclic loading, to evaluate the effect of EM and thermal cyclic loading on the ac behavior of the cable. The ac losses measurements were performed at 2 and 9 T background field and ±0.2 T ac amplitude range from 0.1 to 7 Hz. Fig. 8 shows the total loss per cycle per unit volume of the three types of conductors at 2 T before and after cyclic loading.

Fig. 8 shows that the HFC and LFC conductors exhibit coincident ac loss behavior because the cable pattern and conductor geometry are very close. The ac loss behavior of HFC and

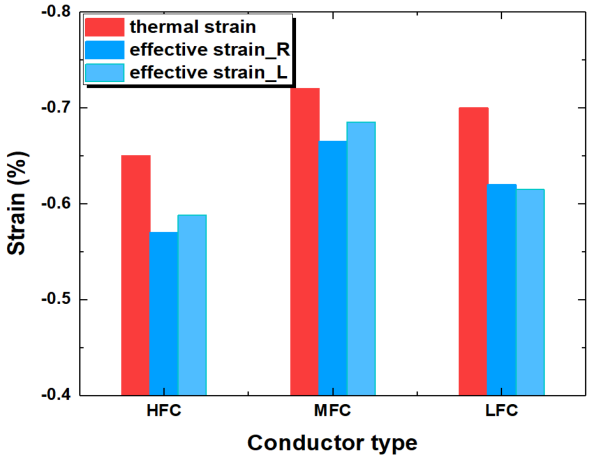

Fig. 7. Comparison between the calculated thermal strain (assuming 100% strain transmission between the jacket and cable) and the measured effective strains of the three types of conductors.

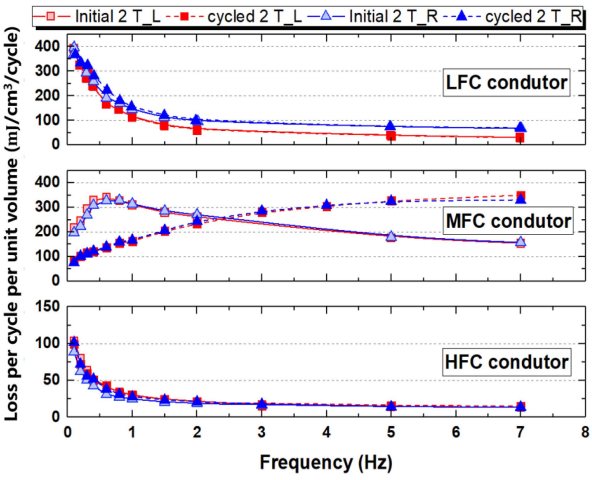

Fig. 8. AC losses per unit volume of the three types of conductors as a function of frequency, before and after EM cyclic loading at 2 T.

LFC conductors are different from that of ITER conductors, only the decreasing part of the curves was measured within the explored frequency range. Similar behavior was observed for the EU-DEMO TF conductor developed by ENEA [11] and the conductor for the HFML 45 T hybrid magnet project [12]. Both conductors are with rectangular cross-section, which indicates that such ac loss behavior could be related to the conductor geometry as well as to the cable pattern [13]. On the other hand, no decrease in ac loss was observed after cyclic loading, indicating that the conductor is very stiff that the cyclic EM load did not alter the interstrand contact resistance, this is in line with the dc test results. But the MFC conductor shows ac loss behavior similar to that of ITER conductors, and in addition, the cyclic EM load affected the ac loss. Except for the difference in the geometry of the cross-section, another remarkable geometrical difference between HFC/LFC conductors and MFC conductor is the void fraction. For the HFC/LFC conductors, the measured void fractions are 28.9% and 29.2%, respectively, which is lower than the designed value. Meanwhile the measured void fraction of MFC conductor is 30.3%, higher than the designed value. This is a possible reason that leads to the different ac loss behaviors of HFC/LFC conductors and MFC conductor. In conclusion, the ac losses depend on the cable geometry, but not on the strand manufacturer.

IV. Conclusion

Three types of cable-in-conduit conductors have been tested successfully in the SULTAN facility for the dc magnet system of the new "Super-X" test facility. High-J_c Nb_3Sn strand is applied on the MFC and HFC conductors. No performance degradation was observed after maximum 150% of nominal cyclic EM loading for each type of conductor, but the WUCD cycle caused a decrease of T_{cs} less than 0.1 K on the MFC conductor made of OST M2007 strand. The effective strain assessment indicates that the EM load on such level (220 kN/m) does not change the strain state of the conductors.

The LFC and HFC conductors show different ac loss behavior to that of ITER conductors, and similar to that of other types of rectangular conductors. The MFC conductor shows ac loss behavior similar to that of ITER conductors, indicating that the ac loss behavior depends on the conductor geometry and cable pattern.

The extrapolated T_{cs} at operating conditions of the three types of conductors can meet the design criterion, which is T_{cs}>5.7 K after 1000 EM cycles. Consequently, the designed parameters of conductor and cable have been qualified and can be frozen for mass manufacturing.

References

[1] H. Han et al., "Structural design of DC magnet for super-X test facility," *IEEE Trans. Appl. Supercond.*, vol. 32, no. 6, Sep. 2022, Art. no. 9500905.
[2] C. Dai et al., "Conceptual design of 15 tesla conductor test facility for future fusion reactor," *IEEE Trans. Appl. Supercond.*, vol. 30, no. 4, Jun. 2020, Art. no. 9500305.
[3] H. Han et al., "Preliminary design of DC magnet for super-X test facility," *IEEE Trans. Appl. Supercond.*, vol. 31, no. 8, Nov. 2021, Art. no. 4901806.
[4] A. Vostner et al., "Development of the EFDA dipole high field conductor," *IEEE Trans. Appl. Supercond.*, vol. 18, no. 2, pp. 544–547, Jun. 2008.
[5] A. Nijhuis, Y. Ilyin, and W. Abbas, "Axial and transverse stress–strain characterization of the EU dipole high current density Nb_3Sn strand," *Supercond. Sci. Technol.*, vol. 21, no. 6, 2008.
[6] W. G. Chen et al., "Final design of the 40 T hybrid magnet superconducting outsert," *IEEE Trans. Appl. Supercond.*, vol. 23, no. 3, Jun. 2013, Art. no. 4300404.
[7] C. Dai et al., "Pre-mature quench study for the high-J_c Nb_3Sn strand," *Intern. Rep.*, 2019.
[8] A. Godeke et al., "A general scaling relation for the critical current density in Nb3Sn," *Supercond. Sci. Technol.*, vol. 19, no. 10, pp. R100–R116, Oct. 2006.
[9] M. Breschi, D. Bessette, and A. Devred, "Evaluation of effective strain and n-value of ITER TF conductor samples," *IEEE Trans. Appl. Supercond.*, vol. 21, no. 3, pp. 1969–1973, Jun. 2011.
[10] N. Mitchell, "Finite element simulations of elasto-plastic processes in Nb_3Sn strands," *Cryogenics*, vol. 45, no. 7, pp. 501–515, 2005.
[11] L. Muzzi et al., "Design, manufacture and test of an 80 kA-class Nb3Sn cable-in-conduit conductor with rectangular geometry and distributed pressure relief channels," *IEEE Trans. Appl. Supercond.*, vol. 27, no. 4, Jun. 2017, Art. no. 4800206.
[12] K. Sedlak et al., "Test of the MF-CICC conductor designed for the 12-T outsert coil of the HFML 45-T hybrid magnet," *IEEE Trans. Appl. Supercond.*, vol. 26, no. 4, Jun. 2016, Art. no. 4300305.
[13] G. Rolando, A. Devred, and A. Nijhuis, "Minimizing coupling loss by selection of twist pitch lengths in multi-stage cable-in-conduit conductors," *Supercond. Sci. Technol.*, vol. 27, no. 1, Jan. 2014, Art. no. 015006.